Author Manuscript

Author Manuscript

Author Manuscript

Author Manuscript

HHS Public Access

Author manuscript

J Neurogenet. Author manuscript; available in PMC 2019 December 01.

Published in final edited form as:

J Neurogenet. 2018 December ; 32(4): 336–352. doi:10.1080/01677063.2018.1493479.

Zebrafish expression reporters and mutants reveal that the IgSF cell adhesion molecule Dscamb is required for feeding and survival

Donald P. Julien[1], **Alex W. Chan**[1], **Joshua Barrios**[2], **Jaffna Mathiaparanam**[3], **Adam Douglass**[2], **Marc A. Wolman**[3], and **Alvaro Sagasti**[1,4]

[1]Department of Molecular, Cell and Developmental Biology and Molecular Biology Institute, University of California, Los Angeles, CA 90095

[2]Department of Neurobiology and Anatomy, University of Utah, Salt Lake City, UT 84112

[3]Department of Integrative Biology, University of Madison, Wisconsin, WI 53706

Abstract

Down Syndrome Cell Adhesion Molecules (DSCAMs) are broadly expressed in nervous systems and play conserved roles in programmed cell death, neuronal migration, axon guidance, neurite branching and spacing, and synaptic targeting. However, DSCAMs appear to have distinct functions in different vertebrate animals, and little is known about their functions outside the retina. We leveraged the genetic tractability and optical accessibility of larval zebrafish to investigate the expression and function of a DSCAM family member, *dscamb*. Using targeted genome editing to create transgenic reporters and loss-of-function mutant alleles, we discovered that *dscamb* is expressed broadly throughout the brain, spinal cord, and peripheral nervous system, but is not required for overall structural organization of the brain. Despite the absence of obvious anatomical defects, homozygous *dscamb* mutants were deficient in their ability to ingest food and rarely survived to adulthood. Thus, we have discovered a novel function for *dscamb* in feeding behavior. The mutant and transgenic lines generated in these studies will provide valuable tools for identifying the molecular and cellular bases of these behaviors.

INTRODUCTION

Establishing the circuits underlying perception, movement, and cognition requires the precise arrangement of intricate neuronal arbors and formation of specific synaptic contacts. Creating such complexity and precision requires diverse molecular signals functioning at the local level (Langley, 1895; Lawrence Zipursky & Sanes, 2010; Sperry, 1963). Many diseases of the nervous system manifest in debilitating neurodegenerative and psychiatric symptoms, despite the absence of major brain malformations, suggesting that molecular signals governing the local assembly of neuronal circuits may play critical roles in these conditions.

[4]Correspondence: Alvaro Sagasti (sagasti@mcdb.ucla.edu).

Author Manuscript Author Manuscript Author Manuscript Author Manuscript

The immunoglobulin superfamily (IgSF) of cell adhesion molecules (CAMs) is one of the largest protein families in vertebrates. Their diversity, broad range of binding interactions, and abundant expression in the nervous system (Vaughn & Bjorkman, 1996), make IgSF CAMs ideal candidates for organizing neuronal circuits. One family of IgSF proteins, the Down Syndrome cell adhesion molecules (DSCAMs), has attracted attention due to *DSCAM*'s location on the Down syndrome critical region (DSCR) of chromosome 21 (Yamakawa et al., 1998), trisomy of which causes the disabilities associated with Down syndrome (Delabar et al., 1993; Korenberg et al., 1994; Korenberg, Bradley, & Disteche, 1992). DSCAMs are single-pass transmembrane proteins, with a conserved extracellular arrangement of Ig and fibronectin repeats (Dietmar Schmucker & Chen, 2009). *Drosophila dscam1* has a unique mechanism of alternative splicing, which generates up to 19,008 different extracellular domains that engage in precise homophilic binding (D. Schmucker et al., 2000). This extreme diversity allows *Drosophila* DSCAMs to serve as specificity molecules mediating neurite self-recognition (Hattori, Millard, Wojtowicz, & Zipursky, 2008; Millard & Zipursky, 2008; Dietmar Schmucker, 2007). Vertebrate DSCAMs, *Dscam* and *Dscam-like 1* (*Dscaml1*), are not extensively alternatively spliced, but are broadly expressed in the central nervous system (CNS) and implicated in many aspects of neuronal development, including axon guidance, programmed cell death, cell migration, neurite branching and spacing, synaptic targeting, and synapse formation (Montesinos, 2014).

The functions of vertebrate DSCAMs have been best studied in the well organized circuitry of the retina. In the mouse retina, DSCAM and DSCAML1 are expressed in non-overlapping subtypes of bipolar cells (BCs), amacrine cells (ACs), and retinal ganglion cells (RGCs). Knockout of either gene causes specific subtypes of these cells to aggregate and fasciculate, disrupting cell spacing (Fuerst et al., 2009; Fuerst, Koizumi, Masland, & Burgess, 2008). In these mouse mutants, neurite branches fasciculate with other branches of the same neuron, as well as neighbors of the same subtype, indicating that DSCAMs are required for both self-avoidance and homotypic branch spacing. Similar to their murine counterparts, chick Dscams, and the closely-related Sidekick (Sdk) and Contactin (Cntn) subfamilies, are expressed in distinct retinal subtypes (Yamagata & Sanes, 2008, 2012; Yamagata, Weiner, & Sanes, 2002). Each IgSF protein is enriched in a particular sublamina of the chick inner plexiform layer (IPL) due to mutual innervation from synaptically connected BCs and RGCs, and are required for establishing those specific connections (Yamagata & Sanes, 2008, 2012; Yamagata et al., 2002). In contrast, mouse DSCAMs are broadly localized throughout the IPL (de Andrade, Kunzelman, Merrill, & Fuerst, 2014; de Andrade, Long, Fleming, Li, & Fuerst, 2014; Fuerst et al., 2009) and play a limited role in lamination that varies with genetic background (Fuerst, Bruce, Rounds, Erskine, & Burgess, 2012; Fuerst, Harris, Johnson, & Burgess, 2010; Li et al., 2015). Additional studies are required to compare the similarities and differences of DSCAM functions across vertebrate taxa.

Although DSCAMs have been best studied in the retina, they are also expressed throughout the brain and spinal cord, a feature conserved among vertebrates (K. L. Agarwala et al., 2001; Gillian M. Barlow, Micales, Chen, Lyons, & Korenberg, 2002; Morales Diaz, 2014; Yamakawa et al., 1998; Yimlamai, Konnikova, Moss, & Jay, 2005), but few studies have investigated roles for DSCAMs outside the retina. Analyzing other DSCAM-expressing regions could identify new roles for these proteins. Zebrafish are a promising model for

Author Manuscript Author Manuscript Author Manuscript Author Manuscript

investigating DSCAM functions; their external fertilization and optical transparency facilitates observation of development of the entire brain in living embryos and larvae. The zebrafish genome has three DSCAM family members: *dscama*, *dscamb*, and *dscaml1*. Although *dscama* expression and function has been investigated (Yimlamai et al., 2005), the expression of *dscamb* has only been characterized in the retina (Sun, Galicia, & Stenkamp, 2018), and its function has yet to be interrogated. In this study, we leveraged the genetic tractability of zebrafish to investigate the expression and function of *dscamb*. To characterize *dscamb* expression, we created reporters using CRISPR/Cas9-targeted enhancer traps. To determine its function, we generated *dscamb* loss-of-function mutant lines with the TALEN targeting system. Using these tools, coupled with cellular and behavioral analyses, we identify a critical new role for *dscamb* in feeding and survival.

RESULTS

dscamb mutations impair survival to adulthood, but produce no obvious anatomical defects

To investigate the function of Dscamb in zebrafish neuronal development, we used TALENs to generate loss-of-function mutant lines. We selected two target sites in the coding region of *dscamb*: 1) the translational start codon, and 2) a region in the middle of exon 2 (Figure 1A). We engineered a pair of TALENs flanking each target site (Cermak et al., 2011) and injected mRNAs encoding each TALEN pair into embryos at the 1-cell stage. For each target site, we used Restriction Fragment Length Polymorphisms (RFLPs) and sequencing to identify multiple founders with germline frameshift mutations that generate premature stop codons (Figure 1B). We established four mutant *dscamb* lines with unique mutant alleles—two mutations for each target site: $dscamb^{t1a}$, $dscamb^{t1b}$, $dscamb^{t2a}$, and $dscamb^{t2b}$. We sequenced RT-PCR products from multiple $dscam^{t2a}$ homozygous embryos and verified that the *dscamb* genomic frameshift mutation was integrated into mRNA transcripts (data not shown).

Across both target sites and mutant alleles, we detected no obvious developmental or anatomical defects distinguishing wild-type and homozygous mutant siblings, at least up to 7 days post-fertilization (dpf). However, most homozygous mutants died before reaching sexual maturity (~3 months old). Moreover, heterozygous siblings were significantly underrepresented relative to their wild-type siblings at the same ages (wild-type: heterozygous: homozygous sibling survival: exon 1 mutants = 43:55:1, exon 2 mutants = 45:52:0; wt × het exact multinomial test: exon 1 mutants $p = 0.0317$, exon 2 mutants $p = 0.0093$), suggesting that *dscamb* mutation confers a developmental deficit that impairs survival.

CRISPR/Cas9-directed enhancer trap integration reveals the Dscamb expression pattern

Closer inspection of the tissues expressing Dscamb could pinpoint developmental defects underlying mutant mortality. To identify *dscamb*-expressing cell types and image their development in live embryos, we created a *dscamb* enhancer trap reporter using CRISPR/Cas9-guided mutagenesis to insert a reporter transgene upstream of *dscamb* (Figure 1C) (Kimura, Hisano, Kawahara, & Higashijima, 2014). By integrating the enhancer trap

Author Manuscript Author Manuscript Author Manuscript Author Manuscript

upstream of the mutant allele, we could more readily identify heterozygous and mutant embryos and thus identify loss-of-function phenotypes in *dscamb*-expressing cells. We selected two guide RNA (gRNA) target sites upstream of the *dscamb* locus: 1) gRNA-Et1, located 69bp upstream of the transcriptional initiation site, and 2) gRNA-Et2, located 4bp upstream of the initiation site. *dscamb*-targeting gRNAs were injected into single-cell embryos along with a donor transgene plasmid containing a minimal heatshock promoter driving expression of Gal4FF (Asakawa & Kawakami, 2009), Cas9-encoding mRNA, and a second gRNA to linearize the donor plasmid (Figure 1C). We generated three lines with integrations upstream of the wild-type allele, and one integrated upstream of the *dscamb*^{t2b} mutant allele (Figure 1D–G). Of the wild-type enhancer trap lines, two were integrated at the gRNA-Et1 target site: Et1(dscamb^{wt}:Gal4)^{i}, Et1(dscamb^{wt}:Gal4)^{o}. The remaining wild-type enhancer trap integrated at the sgRNA-Et2 site: Et2(dscamb^{wt}:Gal4). Integration upstream of the mutant allele was at the gRNA-Et1 site: Et1(dscamb^{t2b}:Gal4). With this method, the enhancer trap plasmid can integrate in either forward or reverse orientations, and multiple copies of the plasmid can integrate tandemly at the target site. Previous studies found only minor differences in enhancer trap expression between forward and reverse integration (Kimura et al., 2014). All three gRNA-Et1 enhancer trap lines were integrated in the reverse orientation; the gRNA-Et2 line showed evidence of both reverse and forward integration (Figure 1D–G).

We crossed each enhancer trap line to Tg(5xUAS:GFP) to compare expression at 5 dpf (Figure 1D–G). Expression was similar regardless of target site, suggesting that integration does not disrupt critical regulatory elements and that the orientation of integration has minimal effects on expression. Integrations upstream of the wild-type and mutant alleles also showed similar expression patterns, indicating that *dscamb* mutations do not dramatically alter expression. UAS transgene positional effects were also minimal, as there was little difference in the expression pattern visualized with other UAS lines (UAS:KikGR, UAS:nfsb-mCherry). Since there were no obvious differences between reporter lines, we focused on the mutant enhancer trap line [Et1(dscamb^{t2b}:Gal4)] for most experiments. This allowed us to characterize the expression pattern of Dscamb while comparing development in heterozygous and homozygous mutants.

As a second approach to characterize *dscamb* expression, we generated a BAC transgenic reporter. Specifically, we replaced the start codon in a 40.8 kb BAC spanning the first exon of *dscamb* with a Gal4-containing reporter cassette and integrated this BAC into the genome to generate a stable line: BAC(dscamb:Gal4) (Figure S1A). Although BAC reporter expression was sparser than Et1(dscamb^{t2b}:Gal4), every region with BAC reporter expression was also observed in the enhancer trap, including the retina, otic hair cells, cranial sensory ganglia, the hindbrain, and the spinal cord, further supporting the accuracy of the enhancer trap expression pattern (Figure S1B–G).

The Dscamb enhancer trap is expressed throughout the central nervous system

To characterize expression of Et1(dscamb^{t2b}:Gal4), we crossed Et1(dscamb^{t2b}:Gal4), Tg(5xUAS:GFP) to a pan-neuronal line [Tg(nbt:RFP)], and imaged fish at embryonic (1 dpf) and larval (4–5 dpf) stages. At both stages, GFP was expressed throughout the brain and

Author Manuscript Author Manuscript Author Manuscript Author Manuscript

spinal cord (Figure 2). Although many cells were GFP+/RFP+, we frequently observed cells that were RFP+/GFP-, indicating that dscamb is not expressed in all neurons. Conversely, many cells were RFP-/GFP+, suggesting that either the nbt:RFP transgene incompletely labels neurons or that *dscamb* is also expressed in glial cells. At 4–5 dpf, the enhancer trap was broadly expressed in the forebrain, midbrain, and hindbrain (Figure 2B). In the forebrain, *dscamb* was expressed in the olfactory bulb and other unidentified regions (Figure 3C; additional forebrain expression not shown). GFP+ neurons were also seen in the hindbrain cerebellum and the midbrain optic tectum, where GFP+ neurites spread throughout the tectal neuropil.

In the spinal cord, enhancer trap expression was more abundant ventrally (Figure 2C). GFP+ motor axons exited the spinal cord to innervate trunk muscles from all three zebrafish primary motor neurons (the caudal (CaP), middle (MiP), and rostral (RoP) neurons, data not shown). Somatosensory Rohon-Beard neurons (RBs) in the dorsal spinal cord also expressed the enhancer trap. Crossing the enhancer trap to a reporter for an RB subtype (*BAC[TrpA1b:GFP]*) (Palanca et al., 2013) demonstrated that *dscamb* is expressed in a subtype of RBs partially overlapping with TrpA1b+ RB neurons (Figure 3A,B). Since *Drosophila Dscam1* regulates self-avoidance in touch-sensing neurons (Hughes et al., 2007; Matthews et al., 2007; Soba et al., 2007), we analyzed sensory axon morphology in the skin by injecting the BAC reporter to sparsely label RBs. We did not observe any significant changes in the frequency of axon crossovers, suggesting that zebrafish *dscamb* does not regulate self-avoidance in RBs (Figure S2). More broadly, we did not detect any obvious structural differences in the brain or spinal cord of homozygous mutant animals (Figure 2). We also compared brain and spinal organization of a wild-type enhancer trap reporter [Et2(dscamb^{wt}:Gal4)] to heterozygous and homozygous enhancer trap mutants, but did not detect any obvious anatomical differences (Figure S3).

Dscamb is broadly expressed in the peripheral nervous system

Et1(dscamb^{t2b}:Gal4) was also expressed broadly in the peripheral nervous system (PNS). At 1 dpf, all of the early sensory ganglia, including the trigeminal, anterior and posterior lateral line, octaval/statoacoustic ganglia, and olfactory placode, contained GFP+ cells (Figure 2A). Compared to Tg(nbt:RFP), many cells in sensory ganglia were RFP+/GFP-, suggesting that *dscamb* is expressed in a subtype of these sensory neurons. At larval stages (5 dpf), enhancer trap expression persisted in trigeminal, anterior lateral line, posterior lateral line, statoacoustic, and vagal ganglia (Figure 2B), and was also observed in the glossopharyngeal and facial ganglia (data not shown). Again, GFP expression was only detected in a subset of sensory neurons, although the size of this subset varied between ganglia. We did not detect obvious defects in the composition or organization of sensory ganglia in *dscamb* mutants (Figure 2A,B).

In several sensory systems, enhancer trap expression was detected in both primary sensory neurons and their downstream partners. For example, in addition to the statoacoustic ganglion, GFP+ sensory hair cells were seen in all sensory hair cell (ovHCs) patches of the otic vesicle (the developing inner ear) (Figure 2B). GFP+ axons, likely afferents from the statoacoustic ganglion, were frequently seen coursing into the ovHC patches. No

Author Manuscript Author Manuscript Author Manuscript Author Manuscript

pronounced changes in ovHC patches or innervating GFP+ axons were detected in *dscamb* homozygous mutants.

In the olfactory system, GFP+ neurons were in both primary olfactory receptor neurons (ORNs) and the downstream olfactory bulb (Figure 3C), suggesting that Dscamb might regulate axon guidance or synaptic coupling between these neurons. Since expression in both ORNs and the olfactory bulb made it difficult to discern the morphology of ORN axon terminals, we crossed Et1(dscamb^{t2b}:Gal4) to a UAS line expressing a photoconvertible fluorescent protein (KikGR) (Figure 3C) (Das & Gage Crump, 2012). Using a UV laser, we selectively photoconverted KikGR from green to red in the ORNs, allowing us to distinguish their axons in the olfactory bulb. Mutant axons innervated the olfactory bulb and coalesced into glomeruli in a pattern closely resembling their heterozygous siblings, indicating that *dscamb* is dispensable for ORN axon guidance and segregation into glomeruli.

Outside of cranial sensory ganglia, Et1(dscamb^{t2b}:Gal4) was expressed in enteric neurons (ENS neurons) scattered along the length of the gut tube (Figure 2C). Coexpression analysis with nbt:RFP revealed that the enhancer was expressed in some, but not all, ENS neurons (Figure 3D). We found no difference in the median number of ENS cells between heterozygous and homozygous mutant embryos (median = 10 ENS neurons in both cases; n = 10 animals per genotype) (Figure 3E), indicating that *dscamb* is not required for the migration of ENS neurons into the distal gut in zebrafish.

Dscamb expression in branchiomotor neurons and their target muscles—At larval stages, the *dscamb* enhancer trap labeled a specific population of muscle fibers, located anterior and ventral to the otic vesicle, including the levator arcus palatini (LEV-AP), dilatator operculi (DIL-OP), adductor hyomandibulae (AD-HYO), levator operculi (LEV-OP), and adductor operculi (AD-OP) (Figure 2B). Additional GFP+ muscle fibers were located on the ventral surface of the head, including the intermandibularis anterior (INTM-A), intermandibularis posterior (INTM-P), interhyoideus (INTE), hyoideus inferior (HH-INF), hyoideus superior (HHSUP), sternohyoideus (SH), adductor mandibulae (ADM), and the transverse ventralis (TV) (Figure 4A) (Diogo, Hinits, & Hughes, 2008; Schilling & Kimmel, 1997). These muscle fibers receive innervation from either the branchiomotor neurons of the V (trigeminal), VII (facial), IX (glossopharyngeal), or X (vagus) cranial nerves, located in the hindbrain. Together, these motor pools coordinate the movement of the jaw, operculum (bony gill cover), and gills during feeding and gill ventilation (Chandrasekhar, 2004; Hernandez, Patterson, & Devoto, 2005; Schilling & Kimmel, 1997). This is the first report of DSCAM family member expression in skeletal muscle, raising the possibility that *dscamb* may regulate the development of peripheral motor circuits.

Defects in feeding or inspiratory motor coordination provide a plausible explanation for homozygous mutant mortality, leading us to speculate that *dscamb* could be required for the development or maintenance of connections between branchiomotor neurons and their target muscle fibers. To distinguish individual hindbrain motor nuclei, we crossed the enhancer trap to *Tg(isl1:GFP)*, which labels cranial motor neurons (Figure 4B,C). At 4 dpf, enhancer trap-expressing cells were not detected in the trigeminal motor nucleus (data not shown), occasionally in the facial nucleus (Figure 4B), and frequently in the vagus nucleus (Figure

Author Manuscript Author Manuscript Author Manuscript Author Manuscript

4C). Thus, at 4 dpf, *dscamb* is expressed in a subset of facial and vagal branchiomotor neurons. To determine if *dscamb* is required for establishing synapses between branchiomotor neurons and target muscles, we used alpha-bungarotoxin (aBTX) to stain neuromuscular junctions (NMJs) in 7 dpf larvae (Figure 4D,E). Using Et1(dscamb^{t2b}:Gal4) expression to visualize *dscamb*-expressing muscles on the ventral surface of the jaw, we did not detect any pronounced defects in the organization of ventral jaw muscles in *dscamb* mutants (Figure 4A). We quantified the number and volume of aBTX-labeled postsynaptic puncta on the INTM-A and INTM-P muscles of the ventral head (Figure 4D–G). There was no significant difference between heterozygous and homozygous mutants (Mann-Whitney-Wilcoxon test: number of puncta $p = 0.98$, volume of puncta $p = 0.46$; $n = 16$ heterozygous and 13 homozygous), suggesting that *dscamb* is dispensable for forming branchiomotor NMJs, though subtle defects in synaptic development may have eluded our analyses.

Dscamb is not required for retinal lamination, cell, or branch spacing

In the mouse retina, *Dscam* is expressed primarily in RGCs, but also in subtypes of ACs and BCs, whereas *Dscaml1* is expressed in rod PRs and distinct BC, AC, and RGC subtypes in rod retinal circuits (Fuerst et al., 2009). Previous studies, using transcriptomics and in situ hybridization identified *dscamb* expression in the ONL, INL, and RGL (Sun et al., 2018), but the extent of gene expression across the major types of retinal neurons has not been assessed in detail. We characterized *dscamb* enhancer trap expression in retinal cryosections from 5 dpf larvae—a time point at which the retina is stratified and functional (Figure 5). Although GFP expression was brightest and most abundant in PRs, the RGL was also densely labeled (Figure 5A). GFP expression in the inner nuclear layer (INL) was less dense, but GFP+ cells were still visible throughout the INL. Based on cell body location, most GFP + INL neurons appeared to be ACs, but GFP+ BCs and HCs were also observed. Thus, *dscamb* is expressed in all major retinal cell types, but is most broadly expressed in PRs, followed by RGCs and ACs. In the mouse retina, *Dscam* or *Dscaml1* loss-of-function reduces programmed cell death, leading to expansion of the INL and IPL (Fuerst et al., 2009, 2008; Keeley et al., 2012). We did not observe any differences in the number of *dscamb*-expressing cells or thickness of the IPL in heterozygous and homozygous *dscamb* mutants (Figure S4), suggesting that *dscamb* does not regulate programmed cell death.

Dscamb is expressed in subtypes of ACs and RGCs but is not required for their lamination or branch spacing—We used immunofluorescence to further characterize the expression of Et1(dscamb^{t2b}:Gal4) surrounding the IPL (Figure 5B–D). Zebrafish ACs can be located in either the INL or the RGL (as displaced ACs [dACs]). We stained 5 dpf retinal cryosections with 5E11, an antibody labeling all ACs (Figure 5B) (Hyatt, Schmitt, Fadool, & Dowling, 1996; Link, Fadool, Malicki, & Dowling, 2000). GFP +/5E11+ cell were present in both the IPL and RGL, confirming that *dscamb* is expressed in ACs, including dACs. However, many 5E11+ cells on both sides of the IPL were GFP-, suggesting that *dscamb* is expressed in a subpopulation of ACs. Staining retinal cryosections for Parvalbumin (Parv), a marker for an AC subtype on both sides of the IPL (Nevin, Taylor, & Baier, 2008) revealed that *dscamb*-expressing ACs sometimes also expressed Parv (Figure 5C). To determine if *dscamb* is expressed in RGCs, we stained for the pan-RGC marker, Hermes (Figure 5D) (Hörnberg et al., 2013; Zearfoss, Chan, Wu, Kloc, & Etkin, 2004),

Author Manuscript Author Manuscript Author Manuscript Author Manuscript

which demonstrated that the *dscamb* enhancer trap labels a subtype of RGCs. There were no appreciable changes in cell number or organization of RGCs or ACs in homozygous mutant retinas (Figure S4C–H).

In both mice and chicks, DSCAMs regulate the segregation of neuronal processes into distinct sublamina in the IPL (Li et al., 2015; Yamagata & Sanes, 2008). In the zebrafish retina, Parv+ processes segregate into three distinct sublaminae: s25, s45, and s85 (Figure 5E) (Nevin et al., 2008). These bands corresponded to the stratification of processes from Dscamb-expressing cells (Figure 5E). s25, the thickest Parv+ band, located closest to the RGL, often co-labeled with GFP+ processes. The Parv+ s45 layer, was flanked by two GFP+ bands. Interestingly, GFP was not expressed in s45, suggesting that this sublamina is composed primarily of processes from GFP- Parv+ ACs. s85, the Parv+ sublamina closest to the INL, was frequently co-labeled with GFP. Although we did not discern defects in the localization of these bands in *dscamb* homozygous mutants (Figure 5F,G), the absence and aggregation of Dscamb-expressing processes into consistent, identifiable sublaminae suggests that Dscamb expression is specific to certain cells types that synapse in specific regions of the IPL.

In mice, *Dscam* and *Dscaml1* mutant AC and RGC neurites fail to self-avoid, leading to extensive fasciculation and an obvious disruption of arbor morphology (Fuerst et al., 2009, 2008). To determine if *dscamb* regulates self-avoidance in the zebrafish retina, we analyzed individual cells in homozygous and heterozygous mutant retinas (Figure 6). To distinguish individual neurons, we sparsely labeled the retina by injecting low concentrations of UAS transgene into Et1(dscamb^{t2b}:Gal4) embryos. At 5dpf GFP+ ACs and RGCs were indistinguishable between heterozygous and homozygous mutants. Although we could not reliably resolve fine details of arbor morphology, we saw no signs of extensive fasciculation resembling the self-avoidance phenotype in mouse DSCAM mutants (Figure 6E–H). Thus, we found no evidence that *dscamb* is required for self-avoidance in the RGC or AC neurites, but cannot rule out that it may play a subtle role in this process.

Dscamb loss-of-function does not disrupt ribbon synapses or mosaic spacing of PRs—Both PRs and ovHCs have specialized synaptic structures called ribbon synapses. Enhancer trap expression in both these cell types raised the intriguing possibility that Dscamb may regulate ribbon synapse development. In *Dscaml1* mutant mice, rod PRs showed defects in synaptic maturation, such as an overabundance of synaptic vesicles and rudimentary synaptic ribbons (Fuerst et al., 2009). Using transmission electron microscopy (TEM), we analyzed the structure of PR synaptic ribbons in 7dpf mutant larvae (Figure S5), focusing on cone synaptic peduncles, because they are easy to identify by the presence of multiple synaptic ribbons. *dscamb* mutant cones developed synaptic ribbons that were indistinguishable from synapses in wild-type retinas.

In *Dscam* and *Dscaml1* mutant mice, cells of the same subtype clump together, disrupting their mosaic spacing (Fuerst et al., 2009, 2008). Zebrafish PRs also have a highly regular mosaic arrangement (Bilotta & Saszik, 2001). To evaluate PR mosaic spacing, we imaged retinas from 7 dpf larvae stained for zpr3, a rod marker in embryonic and larval fish (Larison & Bremiller, 1990), and zpr1, a red and green cone marker (Figure 6A–D) (Schmitt &

Author Manuscript Author Manuscript Author Manuscript Author Manuscript

Dowling, 1996). Both zpr1 and zpr3 were completely coexpressed with Et1(dscamb^{t2b}:Gal4), and GFP+ cells covered the entire PR cell layer, indicating that Dscamb is expressed in all zebrafish PRs. However, the arrangement of rod and cone PRs were indistinguishable between heterozygous and homozygous *dscamb* mutant retinas, suggesting that Dscamb is not required for PR mosaic spacing.

dscamb mutants have largely normal somatosensation and hearing, but may have subtle defects in vision

dscamb is expressed in trigeminal and RB neurons at early developmental stages, when these sensory neurons first innervate the skin. To analyze somatosensory function, we recorded the escape behavior of 2 dpf embryos in response to three trials of light tail touches (Figure 7A). There was no statistically significant difference in touch responses between wild-type, heterozygous, and homozygous mutant larvae (Fisher's exact test of independence $p = 0.4$), indicating that *dscamb* is not required for touch sensation in zebrafish larvae.

To characterize auditory function in larval *dscamb* mutants, we used a prepulse inhibition (PPI) assay. In PPI, an initial weak auditory stimulus inhibits behavioral response to a second stronger stimulus (Bhandiwad, Zeddies, Raible, Rubel, & Sisneros, 2013; Burgess & Granato, 2007b). 6–8 dpf larvae displayed no significant differences in PPI between wild-type, heterozygous, and homozygous mutant embryos (Figure 7B) (ANOVA: $p = 0.98$). The latency of the c-bend responses was also similar between genotypes (ANOVA: $p = 0.46$), indicating that *dscamb* is not required for auditory function or gross motor function.

To assess visual function in *dscamb* mutants, we first analyzed visually-mediated background adaptation (VBA)—a process in which larvae lighten their pigmentation in response to a bright environment and darken it in a low-light environment (Neuhauss et al., 1999). Similar proportions of wild-type, heterozygous, and homozygous mutants adjusted their pigmentation when moved from a dark to light environment (Figure 7C) (light-adapted: wild-type = 63%, heterozygous = 73%, homozygous = 74%; Fisher's exact test: $p = 0.725$). We next tested mutants for the optomotor response (OMR), a behavior in which laval fish tend to swim in the direction of a moving stimulus (Fleisch & Neuhauss, 2006). Heterozygous and homozygous *dscamb* mutants showed similar OMRs to multiple rounds of a rotating stimulus (Figure 7D). These analyses suggest that *dscamb* mutants detect light and that visual circuitry is sufficiently intact to process visual motion.

As a third analysis of visual function, we measured the responsiveness of mutant larvae to changes in illumination (Figure 7E,F). Exposing larvae to abrupt increases ("light flashes") or decreases ("dark flashes") in illumination elicits distinct turning behaviors. Dark-flash responses ("O-bends") have a larger turn angle than light-flash responses ("routine turns") (Burgess & Granato, 2007a). These responses are highly stereotyped and thus provide a sensitive measure of visual function and the circuitry underlying these behaviors. Among *dscamb* genotypes, there were no significant differences in the proportion of 5 dpf larvae that responded to light and dark flash stimuli (Figure 7E1,F1). However, homozygous mutants showed a statistically significant increase in their latency to initiate light-flash responses and a significant decrease in their latency to initiate dark-flash responses (Figure

Author Manuscript Author Manuscript Author Manuscript Author Manuscript

7E2,F2). Other kinematic parameters of these light- and dark-elicited responses, such as distance moved or turning angle (data not shown), were indistinguishable among genotypes, suggesting that mutant behavioral changes are not secondary to motor defects. Thus, *dscamb* mutants likely have subtle deficiencies in initiating visually evoked behaviors.

dscamb mutants die during the first month of life and feed defectively

In the absence of marked sensory defects, a detailed characterization of *dscamb* mutant mortality might point to underlying mechanisms. By comparing the proportion of wild-type, heterozygous, and homozygous mutant siblings to the theoretical Mendelian inheritance, we found a gradual, downward trend in the survival of homozygous mutants, which first reached statistical significance at 16 dpf (Fisher's exact test: $p = 0.0455$) (Figure 8A). By 34 and 60 dpf there were significantly fewer mutants ($p = 0.0013$, $p = 0.0017$, respectively), and no homozygous mutants survived to 60 dpf in this experiment.

Zebrafish larvae begin acquiring nutrients from exogenous food sources at ~7 dpf, when the yolk sac is completely absorbed. In the absence of food, larvae perish from starvation, starting around 10 dpf, and completely succumb by 15 dpf (Versonnen, Roose, Monteyne, & Janssen, 2004; Wilson, 2012). Since *dscamb* mutants were under-represented at 16 dpf, we hypothesized that *dscamb* mutants may have a deficit in either finding or capturing food. To assess food intake, 7 dpf zebrafish larvae were fed larval food coated with fluorescent microspheres. After 90 minutes food content in the foregut (anterior intestine) was assessed (Figure 8B–D) (Field, Kelley, Martell, Goldstein, & Serluca, 2009). wild-type and heterozygous mutants had a similar ability to ingest food (Fisher's exact test, Bonferroni-corrected: wt × het: $p = 0.807$), but four-fold more mutants than wild-type animals had empty foreguts (12.5% vs 46.5%), and five-fold fewer mutants than wild-type had full foreguts (15.1% vs 76.8%) (Fisher's exact test, Bonferroni-corrected: wt × mut: $p < 0.001$, het × mut: $p < 0.001$) (Figure 8D). Since Dscamb is expressed in jaw muscles, we considered the possibility that mutant jaw movements were defective, but a spontaneous "gulping" assay demonstrated that mutant animals were capable of opening their jaws (Figure 8E). Alternatively, mutant animals may have an increased rate of food evacuation from the intestine, but time-lapse imaging of two animals with full guts did not reveal obvious defects in gut transit (data not shown). Thus, *dscamb* mutant animals may suffer from a combination of subtle defects in sensation, movement, digestion, or appetite that make their feeding behavior less efficient.

DISCUSSION

Using targeted mutagenesis, we generated *dscamb* loss-of-function mutants and uncovered highly penetrant defects in mutant survival and food capture. Enhancer trap reporters for *dscamb* revealed broad expression in the central and peripheral nervous systems, and specific muscles of larval fish. In mouse embryos, *Dscam* also has a broad neuronal expression pattern, similar to zebrafish *dscamb*, including expression in the retina, ventral spinal cord, cerebellum, trigeminal ganglion, olfactory epithelium, olfactory bulb, and enteric nervous system (Kishan Lal Agarwala, Ganesh, Amano, Suzuki, & Yamakawa, 2001; Gillian M. Barlow et al., 2002; G. M. Barlow, Micales, Lyons, & Korenberg, 2001;

Author Manuscript Author Manuscript Author Manuscript Author Manuscript

Yamakawa et al., 1998). However, the similarity between mouse and zebrafish DSCAM family members is not complete. In the retina, for example, both mouse *Dscam* and zebrafish *dscamb* are expressed abundantly in RGCs. However, unlike its murine counterpart, zebrafish *dscamb* is also expressed in photoreceptors. These distinct expression patterns suggest that DSCAM family members may have both overlapping and divergent functions across vertebrate species.

Despite broad neuronal expression and impairments in feeding and survival, we did not identify cellular or structural defects in *dscamb* mutants. Several factors could explain this observation. First, our enhancer trap reporter might not accurately reflect endogenous *dscamb* expression, and thus we did not examine the right neuronal populations. However, the fact that enhancer traps integrated at two sites, as well as a BAC reporter, had similar expression patterns argues against this possibility. Enhancer trap expression in the retina is also consistent with a recent study that identified *dscamb* mRNA expression in the ONL, INL, and RGL using in situ hybridization (Sun et al., 2018). Second, gene expression might be incompletely knocked out in our mutant lines, or alternative splice sites or start codons could countervail frameshift mutations. Homozygous mutant mortality was highly penetrant across mutant lines with mutations at two separate target sites, providing strong evidence that the phenotype was specific to *dscamb*. In the future, generating larger genomic deletions that ablate critical domains could ensure complete loss of function. Third, *dscamb* may be genetically redundant with similar genes, such as *dscama* and *dscaml1*. Although the expression of zebrafish *dscaml1* has not been investigated, in situ hybridization studies of *dscama* found broad expression throughout the brain, spinal cord, and retina, similar to *dscamb* (Yimlamai et al., 2005). Thus, it is possible that *dscama* compensates for *dscamb* loss-of-function. Future studies of *dscama*, *dscamb* double mutants could shed light on genetic interactions between these two genes. Nonetheless, the strong defects in homozygous mutant survival and feeding suggest that any functional redundancy is partial. Finally, *dscamb* may regulate subtle aspects of neuronal development that were undetectable in our anatomical analyses, similar to observations that in *Dscam* mutant mice the overall architecture of the brain is largely preserved (Amano et al., 2009; Maynard & Stein, 2012). An accumulation of subtle developmental insults could lead to a dramatic deficit in a complex behavior such as feeding, which requires the coordinated activity of sensory, motor, and neuroendocrine systems. Although we did not detect dramatic defects with auditory, visual, or somatosensory assays, *dscamb* mutants did show increased latency in startle responses to a light flash and decreased latency responses to a dark flash. Thus, *dscamb* mutants are able to see, but may be deficient in their ability to process or respond to visual stimuli.

Vision is a critical component of larval feeding behavior, as anatomical lesions of the optic tectum abolish larval orientation towards and capture of prey paramecia (Gahtan, Tanger, & Baier, 2005), but other sensory systems likely also contribute. For example, the olfactory system regulates feeding behaviors in fish (Hamdani, Kasumyan, & Døving, 2001), and *dscamb* is expressed in both olfactory receptors neurons and the downstream olfactory bulb. Recent studies also demonstrated that molecular or anatomical ablation of branchiomotor neurons in larval zebrafish impairs food capture in a remarkably similar fashion to *dscamb* loss-of-function (Allen et al., 2017). *dscamb* is expressed in a subpopulation of larval

Author Manuscript Author Manuscript Author Manuscript Author Manuscript

branchiomotor neurons and their target muscles, but we did not detect obvious defects in the development of NMJs. Although mutant larvae are at least capable of opening and closing their mouths during spontaneous gulping, feeding is a complex motor behavior that requires the coordinated movement of the jaws, opercula, and the oral cavity (China & Holzman, 2014). Thus, more detailed kinematic analysis of branchiomotor-mediated movements may identify specific defects. The *dscamb* mutant and transgenic lines created in these studies will provide valuable tools to couple with additional behavioral analyses to unravel the cellular basis for visual and feeding impairments, thus uncovering novel functions for Dscam family proteins in vertebrate neuronal development.

METHODS

Zebrafish

Zebrafish (Danio rerio) were grown at 28.5°C on a 14 h/10 h light/dark cycle. Embryos were raised at 28.5°C in embryo water (0.3 g/L Instant Ocean Salt, 0.1% methylene blue). For live confocal imaging, embryos were treated with phenylthiourea (PTU) at 24 hpf to block pigmentation. All experimental procedures were approved by the Chancellor's Animal Research Care Committee at UCLA.

Supplemental Table 1 summarizes the zebrafish lines used for this study.

TALEN cloning and targeted mutagenesis

For each mutant target site in the *dscamb* locus, two 20 bp TALEN binding sites were selected (exon 1: 5'-TAGCTTGGGGATTGAACGCA-3', 5'-TGGAGAAAGAGAAATGCCAA-3'; exon 2: 5'-TCTACGTTCCAGCTTATATT-3', 5'-TGGAGAACACTACCTCTTGC-3'). A restriction enzyme site between each TALEN pair was used for genotyping by RFLP. TALEN constructs were cloned using Golden Gate assembly (Cermak et al., 2011) and an accompanying plasmid kit from Addgene (Addgene Kit #1000000024). TALEN mRNAs were injected into 1-cell embryos to generate stable mutant lines. See supplemental methods for details of mutant generation and genotyping.

BAC cloning and transgenesis

The BAC(*dscamb*:Gal4) line was created by modifying Ch73–102M15, a 40.8 kb BAC containing the first exon of *dscamb*, 22.3 kb upstream of this exon, and 17.8 kb of the first intron. Using in vitro homologous recombination, a Gal4FF-polyA-Kan cassette was inserted in place of the *dscamb* start codon, according to a previously published protocol (Suster, Abe, Schouw, & Kawakami, 2011). See supplemental methods for details.

Enhancer trap creation and transgenesis

Two gRNA target sites upstream of the *dscamb* transcriptional initiation site were chosen for insertion. gRNAs were generated as previously described (Talbot & Amacher, 2014). A zebrafish codon-optimized Cas9 construct (pCS2-nCas9n, Addgene.org plasmid #47929), flanked by nuclear localization signals was used for mutagenesis (Jao, Wente, & Chen, 2013). See supplemental methods for details on gRNA and Cas9 mRNA synthesis.

Author Manuscript Author Manuscript Author Manuscript Author Manuscript

A plasmid used to generate the enhancer trap donor construct was provided by Shin-Ichi Higashijima (pBluescript-SK-Gbait-Hsp-Gal4FF-BGHpA) (Kimura et al., 2014). After modification, this plasmid was injected into Tg(UAS:GFP), *dscamb*^{t2b} heterozygous embryos at the 1-cell stage, along with 1–5 nl of an injection mix containing Cas9 mRNA (200–300 pg/nl), donor plasmid (10–20 pg/nl), gRNA-Et1/Et2 (20–40 pg/nl), and gRNA-Mbait (20–40 pg/nl). Injected fish were screened for Gal4 expression to established stable enhancer trap lines. PCR was used to confirm enhancer trap integration and orientation. See supplemental methods for details.

Anatomical characterization

Details of RB and ENS characterization, ORN photoconversion, retinal dissection, sparse retinal labeling, and TEM are described in supplemental methods. Larvae were prepared for retinal cryosectioning according to a previously published protocol (Uribe & Gross, 2007).

Immunofluorescence staining was carried out using a previously published protocol (Uribe & Gross, 2007), with some modifications, described in supplementary methods. Supplemental Table 1 summarizes antibodies used for immunofluorescence.

Behavioral assays:

Touch: 2 dpf larvae were subjected to three touch trials. For each trial, a small needle was used to lightly graze the tail, and escape responses were scored. Each touch trial was separated by at least 10 seconds.

Background adaptation: 7 dpf fish were placed in the dark for several hours to allow pigment adaptation before being placed under bright illumination. After 30 minutes, larvae were categorized into either light (correct adaptation) or dark (incorrect adaptation) pigmentation groups.

Hearing: 6–8 dpf fish were placed in custom agarose chambers flooded with E3 solution and imaged with a Pike IEEE 1394b camera (Allied Vision Technologies) at 544 frames per second. Startle stimuli consisted of 10ms, 1 KHz acoustic/vibrational pulses delivered by a speaker mounted directly to the imaging platform 6cm from the dish. Image acquisition and stimulus delivery were driven using custom software written in LabView (National Instruments). For PPI testing, each dish was subjected to fifteen startle-only trials and fifteen PPI trials. PPI trials consisted of a non-startling prepulse followed by a startling stimulus with a 400ms inter-stimulus interval. Startle stimulus amplitude was defined as the lowest amplitude evoking c-bend startle in at least 90% of embryos over six repetitions. Prepulse stimulus amplitude was defined as the highest amplitude evoking c-bend startle behaviors in less than 10% of embryos over six repetitions. Percent inhibition was calculated for each fish as [(% of startle trials showing short-latency C-bends) – (% of PPI trials showing short-latency C-bends)] / (% of startle trials showing short-latency C-bends) * 100.

Optomotor response: 7 dpf fish were transferred to a 35 mm petri dish inside a circular arena lined with arrays of computer-controlled LEDs. Using MatLab software, illumination of LED arrays was coordinated into bars that rotated around the chamber circumference. The angular velocity and direction of the rotating stimuli was adjusted along a 0.05 Hz sine

Author Manuscript Author Manuscript Author Manuscript Author Manuscript

wave. Four larvae, each in their own dish, were tested during each experiment, and their movement was recorded by a camera above the testing chamber. Each change of the stimulus direction was counted as one trial. Swimming behavior was ranked on a 1–3 scale: 3 = movement in the direction of stimulus; 2 = undirected movement; 1 = movement opposite to the stimulus.

Light and dark flash responses: 5 dpf larvae in 60mm Petri dishes (20 fish per dish) were adapted on a white light box (800 μW/cm2) for at least 1 hour prior to testing. Each larva was transferred to a well of a 4×4 testing grid (Wolman, Jain, Liss, & Granato, 2011). Responses to light and dark flash stimuli were recorded with a MotionPro Y4 high-speed video camera (Integrated Design Tools, Tallahassee, FL, USA) at 1,000 frames per second and 512×512 pixel resolution, using a 50mm macro lens (Sigma Corporation of America, Ronkonkoma, NY, USA). Larvae were illuminated from above with a mounted LED light (MCWHL5 6500 K LED, powered by LEDD1B driver, Thorlabs, Newton, New Jersey, USA) and below with an infrared light source (IR Illuminator CM-IR200B, C&M Vision Technologies, Houston, TX, USA). Video images were analyzed for O-bend and routine turn response initiations and kinematics with the FLOTE software package, as previously described (Burgess & Granato, 2007a, 2007b; Burgess, Schoch, & Granato, 2010; Wolman et al., 2011). Dark flash O-bends and light flash turns were elicited and analyzed as previously described (Burgess & Granato, 2007a; Wolman et al., 2011). Once in the testing grid, larvae were acclimated to an overhead light (85 μW/cm2 for dark flashes, 25 μW/cm2 for light flashes) for 5 minutes before exposure to a series of 10 flash stimuli (dark flash = lights off, light flash = light increased to 600 μW/cm2 within 1msec). Each stimulus lasted for 1 second and stimuli was presented at a 30 second interstimulus interval.

After all behavioral tests, individual fish were lysed for genotyping. Thus, the experimenter was blind to genotype during behavioral testing.

Mortality analysis

A mixture of wild-type, heterozygous, and homozygous *dscamb*^{t2b} mutant siblings were distributed into tanks at a density of 20–40 fish/tank and raised under standard rearing conditions. At select time-points (7, 10, 13, 16, 19, 34, and 60 dpf), whole tanks were euthanized in 0.02% tricaine on-ice for 10 min, and individual fish were either lysed whole or fin clipped (34 and 60 dpf only) for genotyping.

Food intake assay

Analysis of food intake was adapted from a previously published protocol (Field et al., 2009). See supplemental methods for details.

Gulping assay

At 7 dpf, Et1(dscamb^{t2b}:Gal4), Tg(UAS:GFP) heterozygous and homozygous mutant siblings were immobilized in 3% methylcellulose, with the ventral side facing up. 20 sec videos of spontaneous jaw movements (or “gulps”) were recorded on an AxioCam MRm CCD camera mounted on SteREO Discovery.V12 dissecting microscope with a frame interval of 0.076 frames/sec. After recording, individual larvae were lysed for genotyping.

Author Manuscript Author Manuscript Author Manuscript Author Manuscript

Videos were analyzed by counting the total number of gulps during each video. The observer was blind to genotype while counting.

Statistical analyses

All statistical analyses were performed using the R software package.

Supplementary Material

Refer to Web version on PubMed Central for supplementary material.

ACKNOWLEDGMENTS

We thank Shin-Ichi Higashijima for the enhancer trap donor plasmid (pBluescript-Gbait-Hsp-Gal4ff-BGHpA), Koichi Kawakami for the Tg(UAS:GFP) line, Anand Chandrasekhar for the the Tg(isl1:GFP) line, Gage Crump for the Tg(UAS:KikGR) line, Robert Modlin for the Tg(nbt:DsRed) line, and Kate Whitlock for advice on olfactory analyses. Anti-Hermes and 5E11 antibodies were generously donated by James Fadool and Malgorzata Kloc, respectively. We thank Marianne Cilluffo of the UCLA Brain Research Institute Electron Microscopy Core Facility for histological processing of larvae for TEM. We also thank Mark Frye for the LED array for OMR analyses. Inspiration for these studies came from preliminary investigations conducted by Fang Wang. DPJ was supported by a scholarship from the Achievement Rewards for College Scientists (ARCS) Foundation and the UCLA Philip Whitcome Predoctoral Training Program in Molecular Biology. This research was supported by a grant to AS from the National Institute of Arthritis and Musculoskeletal and Skin Diseases (R01AR064582).

BIBLIOGRAPHY

Agarwala KL, Ganesh S, Amano K, Suzuki T, & Yamakawa K (2001). DSCAM, a Highly Conserved Gene in Mammals, Expressed in Differentiating Mouse Brain. Biochemical and Biophysical Research Communications, 281(3), 697–705. [PubMed: 11237714]

Agarwala KL, Ganesh S, Tsutsumi Y, Suzuki T, Amano K, & Yamakawa K (2001). Cloning and functional characterization of DSCAML1, a novel DSCAM-like cell adhesion molecule that mediates homophilic intercellular adhesion. Biochemical and Biophysical Research Communications, 285(3), 760–772. [PubMed: 11453658]

Allen JR, Bhattacharyya KD, Asante E, Almadi B, Schafer K, Davis J, … Chandrasekhar A (2017). Role of branchiomotor neurons in controlling food intake of zebrafish larvae. Journal of Neurogenetics, 1–10.

Amano K, Fujii M, Arata S, Tojima T, Ogawa M, Morita N, … Yamakawa K (2009). DSCAM deficiency causes loss of pre-inspiratory neuron synchroneity and perinatal death. The Journal of Neuroscience: The Official Journal of the Society for Neuroscience, 29(9), 2984–2996. [PubMed: 19261893]

Asakawa K, & Kawakami K (2009). The Tol2-mediated Gal4-UAS method for gene and enhancer trapping in zebrafish. Methods, 49(3), 275–281. [PubMed: 19835787]

Barlow GM, Micales B, Chen X-N, Lyons GE, & Korenberg JR (2002). Mammalian DSCAMs: roles in the development of the spinal cord, cortex, and cerebellum? Biochemical and Biophysical Research Communications, 293(3), 881–891. [PubMed: 12051741]

Barlow GM, Micales B, Lyons GE, & Korenberg JR (2001). Down syndrome cell adhesion molecule is conserved in mouse and highly expressed in the adult mouse brain. Cytogenetics and Cell Genetics, 94(3–4), 155–162. [PubMed: 11856873]

Bhandiwad AA, Zeddies DG, Raible DW, Rubel EW, & Sisneros JA (2013). Auditory sensitivity of larval zebrafish (Danio rerio) measured using a behavioral prepulse inhibition assay. The Journal of Experimental Biology, 216(Pt 18), 3504–3513. [PubMed: 23966590]

Bilotta J, & Saszik S (2001). The zebrafish as a model visual system. International Journal of Developmental Neuroscience: The Official Journal of the International Society for Developmental Neuroscience, 19(7), 621–629. [PubMed: 11705666]

Author Manuscript Author Manuscript Author Manuscript Author Manuscript

Burgess HA, & Granato M (2007a). Modulation of locomotor activity in larval zebrafish during light adaptation. The Journal of Experimental Biology, 210(Pt 14), 2526–2539. [PubMed: 17601957]

Burgess HA, & Granato M (2007b). Sensorimotor gating in larval zebrafish. The Journal of Neuroscience: The Official Journal of the Society for Neuroscience, 27(18), 4984–4994. [PubMed: 17475807]

Burgess HA, Schoch H, & Granato M (2010). Distinct retinal pathways drive spatial orientation behaviors in zebrafish navigation. Current Biology: CB, 20(4), 381–386. [PubMed: 20153194]

Cermak T, Doyle EL, Christian M, Wang L, Zhang Y, Schmidt C, … Voytas DF (2011). Efficient design and assembly of custom TALEN and other TAL effector-based constructs for DNA targeting. Nucleic Acids Research, 39(12), e82. [PubMed: 21493687]

Chandrasekhar A (2004). Turning heads: development of vertebrate branchiomotor neurons. Developmental Dynamics: An Official Publication of the American Association of Anatomists, 229(1), 143–161. [PubMed: 14699587]

China V, & Holzman R (2014). Hydrodynamic starvation in first-feeding larval fishes. Proceedings of the National Academy of Sciences of the United States of America, 111(22), 8083–8088. [PubMed: 24843180]

Das A, & Gage Crump J (2012). Bmps and Id2a Act Upstream of Twist1 To Restrict Ectomesenchyme Potential of the Cranial Neural Crest. PLoS Genetics, 8(5), e1002710. [PubMed: 22589745]

de Andrade GB, Kunzelman L, Merrill MM, & Fuerst PG (2014). Developmentally dynamic colocalization patterns of DSCAM with adhesion and synaptic proteins in the mouse retina. Molecular Vision, 20, 1422–1433. [PubMed: 25352748]

de Andrade GB, Long SS, Fleming H, Li W, & Fuerst PG (2014). DSCAM localization and function at the mouse cone synapse. The Journal of Comparative Neurology, 522(11), 2609–2633. [PubMed: 24477985]

Delabar JM, Theophile D, Rahmani Z, Chettouh Z, Blouin JL, Prieur M, … Sinet PM (1993). Molecular mapping of twenty-four features of Down syndrome on chromosome 21. European Journal of Human Genetics: EJHG, 1(2), 114–124. [PubMed: 8055322]

Diogo R, Hinits Y, & Hughes SM (2008). Development of mandibular, hyoid and hypobranchial muscles in the zebrafish: homologies and evolution of these muscles within bony fishes and tetrapods. BMC Developmental Biology, 8(1), 24. [PubMed: 18307809]

Field HA, Kelley KA, Martell L, Goldstein AM, & Serluca FC (2009). Analysis of gastrointestinal physiology using a novel intestinal transit assay in zebrafish. Neurogastroenterology and Motility: The Official Journal of the European Gastrointestinal Motility Society, 21(3), 304–312. [PubMed: 19140958]

Fleisch VC, & Neuhauss SCF (2006). Visual behavior in zebrafish. Zebrafish, 3(2), 191–201. [PubMed: 18248260]

Fuerst PG, Bruce F, Rounds RP, Erskine L, & Burgess RW (2012). Cell autonomy of DSCAM function in retinal development. Developmental Biology, 361(2), 326–337. [PubMed: 22063212]

Fuerst PG, Bruce F, Tian M, Wei W, Elstrott J, Feller MB, … Burgess RW (2009). DSCAM and DSCAML1 function in self-avoidance in multiple cell types in the developing mouse retina. Neuron, 64(4), 484–497. [PubMed: 19945391]

Fuerst PG, Harris BS, Johnson KR, & Burgess RW (2010). A novel null allele of mouse DSCAM survives to adulthood on an inbred C3H background with reduced phenotypic variability. Genesis, 48(10), 578–584. [PubMed: 20715164]

Fuerst PG, Koizumi A, Masland RH, & Burgess RW (2008). Neurite arborization and mosaic spacing in the mouse retina require DSCAM. Nature, 451(7177), 470–474. [PubMed: 18216855]

Gahtan E, Tanger P, & Baier H (2005). Visual prey capture in larval zebrafish is controlled by identified reticulospinal neurons downstream of the tectum. The Journal of Neuroscience: The Official Journal of the Society for Neuroscience, 25(40), 9294–9303. [PubMed: 16207889]

Hamdani EH, Kasumyan A, & Døving KB (2001). Is feeding behaviour in crucian carp mediated by the lateral olfactory tract? Chemical Senses, 26(9), 1133–1138. [PubMed: 11705798]

Hattori D, Millard SS, Wojtowicz WM, & Zipursky SL (2008). Dscam-mediated cell recognition regulates neural circuit formation. Annual Review of Cell and Developmental Biology, 24, 597–620.

Author Manuscript Author Manuscript Author Manuscript Author Manuscript

Hernandez LP, Patterson SE, & Devoto SH (2005). The development of muscle fiber type identity in zebrafish cranial muscles. Anatomy and Embryology, 209(4), 323–334. [PubMed: 15761723]

Hörnberg H, Wollerton-van Horck F, Maurus D, Zwart M, Svoboda H, Harris WA, & Holt CE (2013). RNA-binding protein Hermes/RBPMS inversely affects synapse density and axon arbor formation in retinal ganglion cells in vivo. The Journal of Neuroscience: The Official Journal of the Society for Neuroscience, 33(25), 10384–10395. [PubMed: 23785151]

Hughes ME, Bortnick R, Tsubouchi A, Bäumer P, Kondo M, Uemura T, & Schmucker D (2007). Homophilic Dscam interactions control complex dendrite morphogenesis. Neuron, 54(3), 417–427. [PubMed: 17481395]

Hyatt GA, Schmitt EA, Fadool JM, & Dowling JE (1996). Retinoic acid alters photoreceptor development in vivo. Proceedings of the National Academy of Sciences of the United States of America, 93(23), 13298–13303. [PubMed: 8917585]

Jao L-E, Wente SR, & Chen W (2013). Efficient multiplex biallelic zebrafish genome editing using a CRISPR nuclease system. Proceedings of the National Academy of Sciences of the United States of America, 110(34), 13904–13909. [PubMed: 23918387]

Keeley PW, Sliff BJ, Lee SCS, Fuerst PG, Burgess RW, Eglen SJ, & Reese BE (2012). Neuronal clustering and fasciculation phenotype in Dscam- and Bax-deficient mouse retinas. The Journal of Comparative Neurology, 520(7), 1349–1364. [PubMed: 22396220]

Kimura Y, Hisano Y, Kawahara A, & Higashijima S-I (2014). Efficient generation of knock-in transgenic zebrafish carrying reporter/driver genes by CRISPR/Cas9-mediated genome engineering. Scientific Reports, 4, 6545. [PubMed: 25293390]

Korenberg JR, Bradley C, & Disteche CM (1992). Down syndrome: molecular mapping of the congenital heart disease and duodenal stenosis. American Journal of Human Genetics, 50(2), 294–302. [PubMed: 1531166]

Korenberg JR, Chen XN, Schipper R, Sun Z, Gonsky R, Gerwehr S, … Disteche C (1994). Down syndrome phenotypes: the consequences of chromosomal imbalance. Proceedings of the National Academy of Sciences of the United States of America, 91(11), 4997–5001. [PubMed: 8197171]

Langley JN (1895). Note on Regeneration of Prae-Ganglionic Fibres of the Sympathetic. The Journal of Physiology, 18(3), 280–284.

Larison KD, & Bremiller R (1990). Early onset of phenotype and cell patterning in the embryonic zebrafish retina. Development, 109(3), 567–576. [PubMed: 2401210]

Lawrence Zipursky S, & Sanes JR (2010). Chemoaffinity Revisited: Dscams, Protocadherins, and Neural Circuit Assembly. Cell, 143(3), 343–353. [PubMed: 21029858]

Link BA, Fadool JM, Malicki J, & Dowling JE (2000). The zebrafish young mutation acts non-cell-autonomously to uncouple differentiation from specification for all retinal cells. Development, 127(10), 2177–2188. [PubMed: 10769241]

Li S, Sukeena JM, Simmons AB, Hansen EJ, Nuhn RE, Samuels IS, & Fuerst PG (2015). DSCAM promotes refinement in the mouse retina through cell death and restriction of exploring dendrites. The Journal of Neuroscience: The Official Journal of the Society for Neuroscience, 35(14), 5640–5654. [PubMed: 25855178]

Matthews BJ, Kim ME, Flanagan JJ, Hattori D, Clemens JC, Zipursky SL, & Grueber WB (2007). Dendrite self-avoidance is controlled by Dscam. Cell, 129(3), 593–604. [PubMed: 17482551]

Maynard KR, & Stein E (2012). DSCAM contributes to dendrite arborization and spine formation in the developing cerebral cortex. The Journal of Neuroscience: The Official Journal of the Society for Neuroscience, 32(47), 16637–16650. [PubMed: 23175819]

Millard SS, & Zipursky SL (2008). Dscam-mediated repulsion controls tiling and self-avoidance. Current Opinion in Neurobiology, 18(1), 84–89. [PubMed: 18538559]

Montesinos ML (2014). Roles for DSCAM and DSCAML1 in central nervous system development and disease. Advances in Neurobiology, 8, 249–270. [PubMed: 25300140]

Morales Diaz HD (2014). Down syndrome cell adhesion molecule is important for early development in Xenopus tropicalis. Genesis, 52(10), 849–857. [PubMed: 25088188]

Neuhauss SC, Biehlmaier O, Seeliger MW, Das T, Kohler K, Harris WA, & Baier H (1999). Genetic disorders of vision revealed by a behavioral screen of 400 essential loci in zebrafish. The Journal

Author Manuscript Author Manuscript Author Manuscript Author Manuscript

of Neuroscience: The Official Journal of the Society for Neuroscience, 19(19), 8603–8615. [PubMed: 10493760]

Nevin LM, Taylor MR, & Baier H (2008). Hardwiring of fine synaptic layers in the zebrafish visual pathway. Neural Development, 3, 36. [PubMed: 19087349]

Palanca AMS, Lee S-L, Yee LE, Joe-Wong C, Trinh LA, Hiroyasu E, … Sagasti A (2013). New transgenic reporters identify somatosensory neuron subtypes in larval zebrafish. Developmental Neurobiology, 73(2), 152–167. [PubMed: 22865660]

Schilling TF, & Kimmel CB (1997). Musculoskeletal patterning in the pharyngeal segments of the zebrafish embryo. Development, 124(15), 2945–2960. [PubMed: 9247337]

Schmitt EA, & Dowling JE (1996). Comparison of topographical patterns of ganglion and photoreceptor cell differentiation in the retina of the zebrafish, Danio rerio. The Journal of Comparative Neurology, 371(2), 222–234. [PubMed: 8835728]

Schmucker D (2007). Molecular diversity of Dscam: recognition of molecular identity in neuronal wiring. Nature Reviews. Neuroscience, 8(12), 915–920. [PubMed: 18026165]

Schmucker D, & Chen B (2009). Dscam and DSCAM: complex genes in simple animals, complex animals yet simple genes. Genes & Development, 23(2), 147–156. [PubMed: 19171779]

Schmucker D, Clemens JC, Shu H, Worby CA, Xiao J, Muda M, … Zipursky SL (2000). Drosophila Dscam is an axon guidance receptor exhibiting extraordinary molecular diversity. Cell, 101(6), 671–684. [PubMed: 10892653]

Soba P, Zhu S, Emoto K, Younger S, Yang S-J, Yu H-H, … Jan Y-N (2007). Drosophila sensory neurons require Dscam for dendritic self-avoidance and proper dendritic field organization. Neuron, 54(3), 403–416. [PubMed: 17481394]

Sperry RW (1963). CHEMOAFFINITY IN THE ORDERLY GROWTH OF NERVE FIBER PATTERNS AND CONNECTIONS. Proceedings of the National Academy of Sciences of the United States of America, 50, 703–710. [PubMed: 14077501]

Sun C, Galicia C, & Stenkamp DL (2018). Transcripts within rod photoreceptors of the Zebrafish retina. BMC Genomics, 19(1), 127. [PubMed: 29422031]

Suster ML, Abe G, Schouw A, & Kawakami K (2011). Transposon-mediated BAC transgenesis in zebrafish. Nature Protocols, 6(12), 1998–2021. [PubMed: 22134125]

Talbot JC, & Amacher SL (2014). A streamlined CRISPR pipeline to reliably generate zebrafish frameshifting alleles. Zebrafish, 11(6), 583–585. [PubMed: 25470533]

Uribe RA, & Gross JM (2007). Immunohistochemistry on Cryosections from Embryonic and Adult Zebrafish Eyes. Cold Spring Harbor Protocols, 2007(7), db.prot4779.

Vaughn DE, & Bjorkman PJ (1996). The (Greek) key to structures of neural adhesion molecules. Neuron, 16(2), 261–273. [PubMed: 8789942]

Versonnen BJ, Roose P, Monteyne EM, & Janssen CR (2004). Estrogenic and toxic effects of methoxychlor on zebrafish (Danio rerio). Environmental Toxicology and Chemistry / SETAC, 23(9), 2194–2201.

Wilson C (2012). Aspects of larval rearing. ILAR Journal / National Research Council, Institute of Laboratory Animal Resources, 53(2), 169–178.

Wolman MA, Jain RA, Liss L, & Granato M (2011). Chemical modulation of memory formation in larval zebrafish. Proceedings of the National Academy of Sciences of the United States of America, 108(37), 15468–15473. [PubMed: 21876167]

Yamagata M, & Sanes JR (2008). Dscam and Sidekick proteins direct lamina-specific synaptic connections in vertebrate retina. Nature, 451(7177), 465–469. [PubMed: 18216854]

Yamagata M, & Sanes JR (2012). Expanding the Ig superfamily code for laminar specificity in retina: expression and role of contactins. The Journal of Neuroscience: The Official Journal of the Society for Neuroscience, 32(41), 14402–14414. [PubMed: 23055510]

Yamagata M, Weiner JA, & Sanes JR (2002). Sidekicks: synaptic adhesion molecules that promote lamina-specific connectivity in the retina. Cell, 110(5), 649–660. [PubMed: 12230981]

Yamakawa K, Huot YK, Haendelt MA, Hubert R, Chen XN, Lyons GE, & Korenberg JR (1998). DSCAM: a novel member of the immunoglobulin superfamily maps in a Down syndrome region and is involved in the development of the nervous system. Human Molecular Genetics, 7(2), 227–237. [PubMed: 9426258]

Author Manuscript Author Manuscript Author Manuscript Author Manuscript

Yimlamai D, Konnikova L, Moss LG, & Jay DG (2005). The zebrafish down syndrome cell adhesion molecule is involved in cell movement during embryogenesis. Developmental Biology, 279(1), 44–57. [PubMed: 15708557]

Zearfoss NR, Chan AP, Wu CF, Kloc M, & Etkin LD (2004). Hermes is a localized factor regulating cleavage of vegetal blastomeres in Xenopus laevis. Developmental Biology, 267(1), 60–71. [PubMed: 14975717]

Author Manuscript Author Manuscript Author Manuscript Author Manuscript

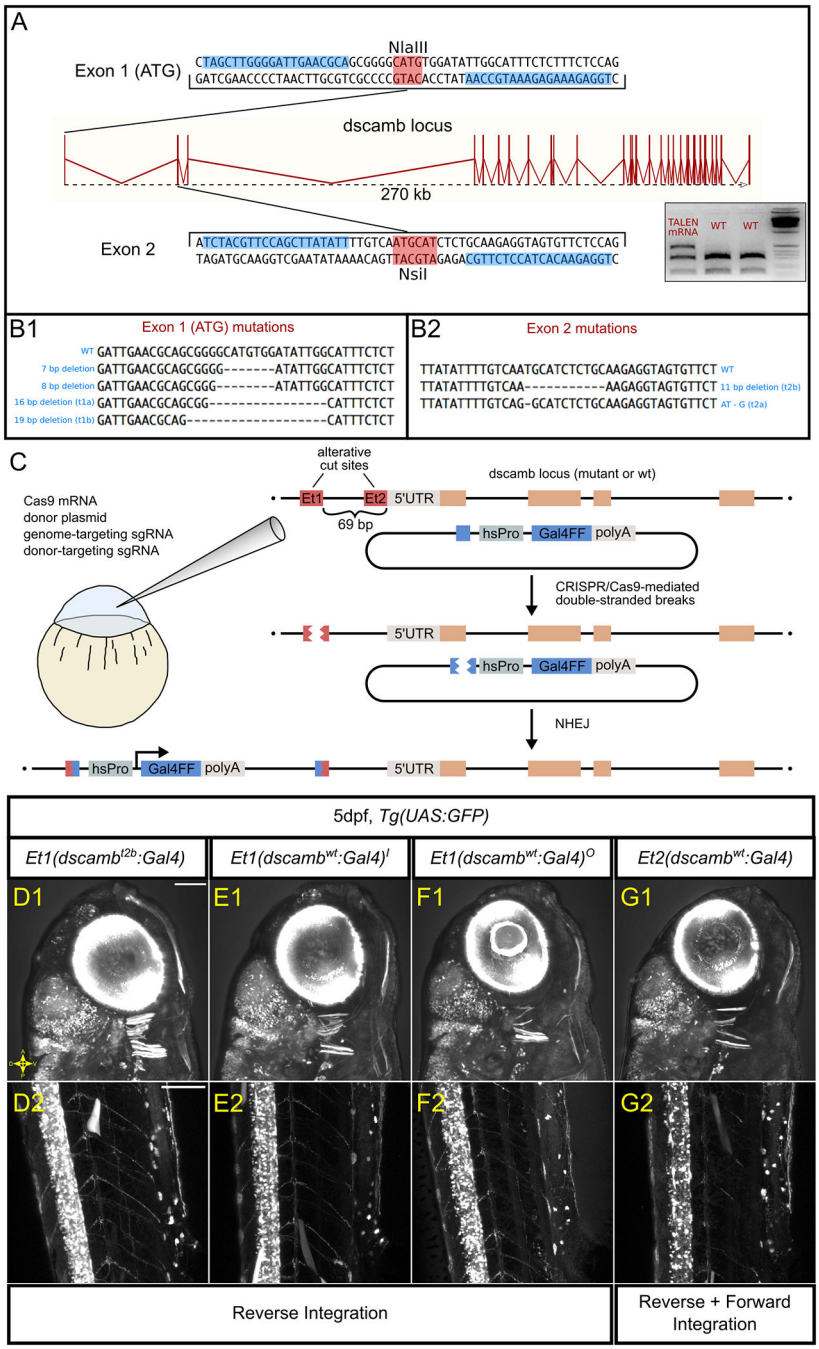

Figure 1 –. Using targeted mutagenesis to generate *dscamb* loss-of-function mutants and enhancer trap reporters

A) The *dscamb* locus, including TALEN target sites in exon 1 (top) and exon 2 (bottom). Blue boxes indicate TALEN binding sites. Red boxes indicate restriction enzyme sites used for RFLP genotyping. Inset is an example of RFLP genotyping for mutations at exon 2 using genomic DNA from pooled embryos injected with TALEN-encoding mRNA or uninjected. The upper, uncut band in TALEN-injected embryos indicates mutation of the NsiI site. Gene diagram adapted from Ensembl.

B) TALEN-generated germline mutations at exon 1 (B1) and exon 2 (B2) sites.

C) CRISPR/Cas9 strategy for enhancer trap insertion.
D-G) Representative confocal images of independent enhancer trap lines, showing reporter expression in the head (D1, E1, F1, G1) and trunk (D2, E2, F2, G2). Scale bars = 100 um.

Author Manuscript Author Manuscript Author Manuscript Author Manuscript

Author Manuscript Author Manuscript Author Manuscript Author Manuscript

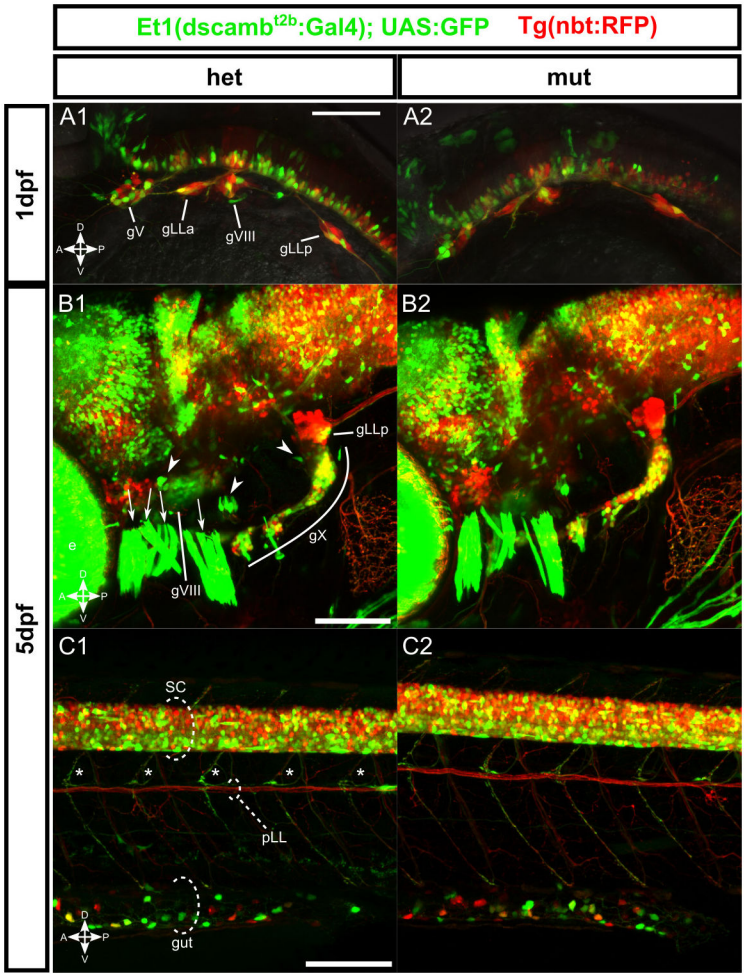

Figure 2 –. *dscamb* enhancer trap reporter is expressed broadly throughout the CNS and PNS, but homozygous mutant embryos lack obvious structural defects

A-C) Et1(dscamb^{t2b}:Gal4) enhancer trap (green) crossed to pan-neuronal Tg(nbt:RFP) in heterozygous (left) and homozygous (right) mutants.

A1, A2) Lateral view of the head in 1dpf embryos. gV: trigeminal ganglion, gLLa: anterior lateral line ganglion, gVIII: statoacoustic ganglion, gLLp: posterior lateral line ganglion.

B1, B2) Lateral view of head in 5dpf larvae. e: eye, gVIII: statoacoustic ganglion, gX: vagal ganglia, gLLp: posterior lateral line ganglion, arrowheads: otic vesicle hair cell patches, arrows: jaw muscles.

C1, C2) Lateral view of trunk in 5dpf larvae. SC: spinal cord, pLL: posterior lateral line axons, asterisks: motor neuron axons, gut: intestine.

Scale bars: 100μm.

Author Manuscript Author Manuscript Author Manuscript Author Manuscript

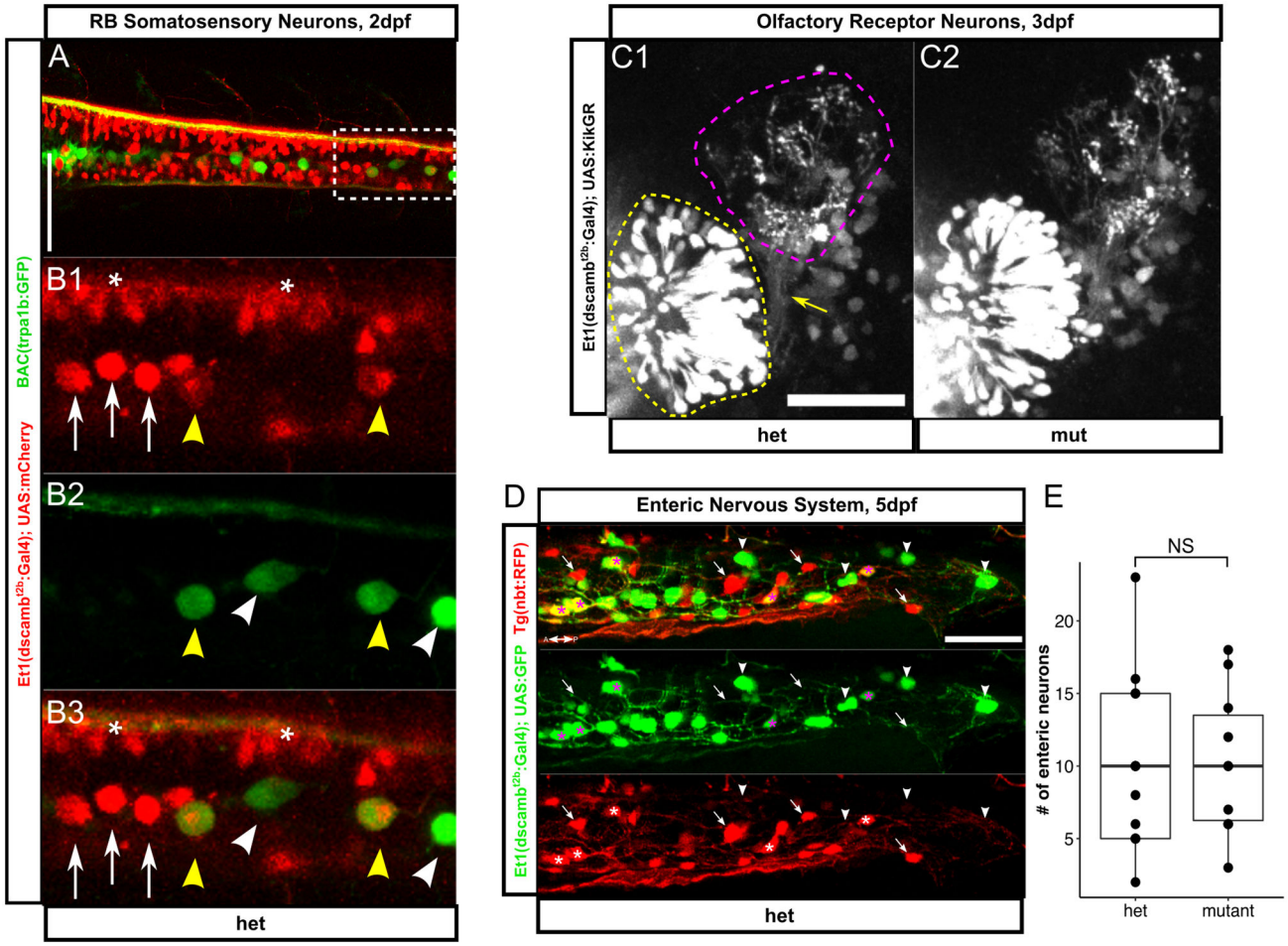

Figure 3 –. *dscamb* expression and function in specialized cell types

A) Dorsal view of spinal cord in 2dpf embryo showing Et1(dscamb^{t2b}:Gal4) in red and BAC(trpa1b:GFP) in green. Scale bar: 100μm. Anterior is to the left.

B1-B3) Higher magnification of box in A. Yellow arrowheads: GFP+/RFP+ RBs, white arrowheads: GFP+/RFP-RBs, white arrows: GFP-/RFP+ RBs, asterisks: other RFP+ neurons.

C) Et1(dscamb^{t2b}:Gal4) driving expression of KikGR in 3dpf heterozygous (C1) and homozygous (C2) larvae. KikGR in ORNs (yellow dashed region) was photoconverted from green to red to delineate axon terminals in glomeruli (magenta dashed region). Yellow arrow: ORN axon coursing to the olfactory bulb. Scale bar: 50μm. Dorsal is up, medial is right.

D) Distal portion of gut in a 5dpf heterozygous dscamb mutant; Et1(dscamb^{t2b}:Gal4) expression in green and Tg(nbt:RFP) expression in red. Asterisks: GFP+/RFP+ enteric neurons, arrowheads: GFP+ only enteric neurons, arrows: RFP+ only enteric neurons. Scale bar: 50μm

E) Number of enteric neurons in the terminal 250μm of the gut. Each point represents one larvae. Mann-Whitney-Wilcoxon test: p = 0.68. Middle box line is the median; lower and upper ends of boxes are 25th and 75th percentiles.

Author Manuscript Author Manuscript Author Manuscript Author Manuscript

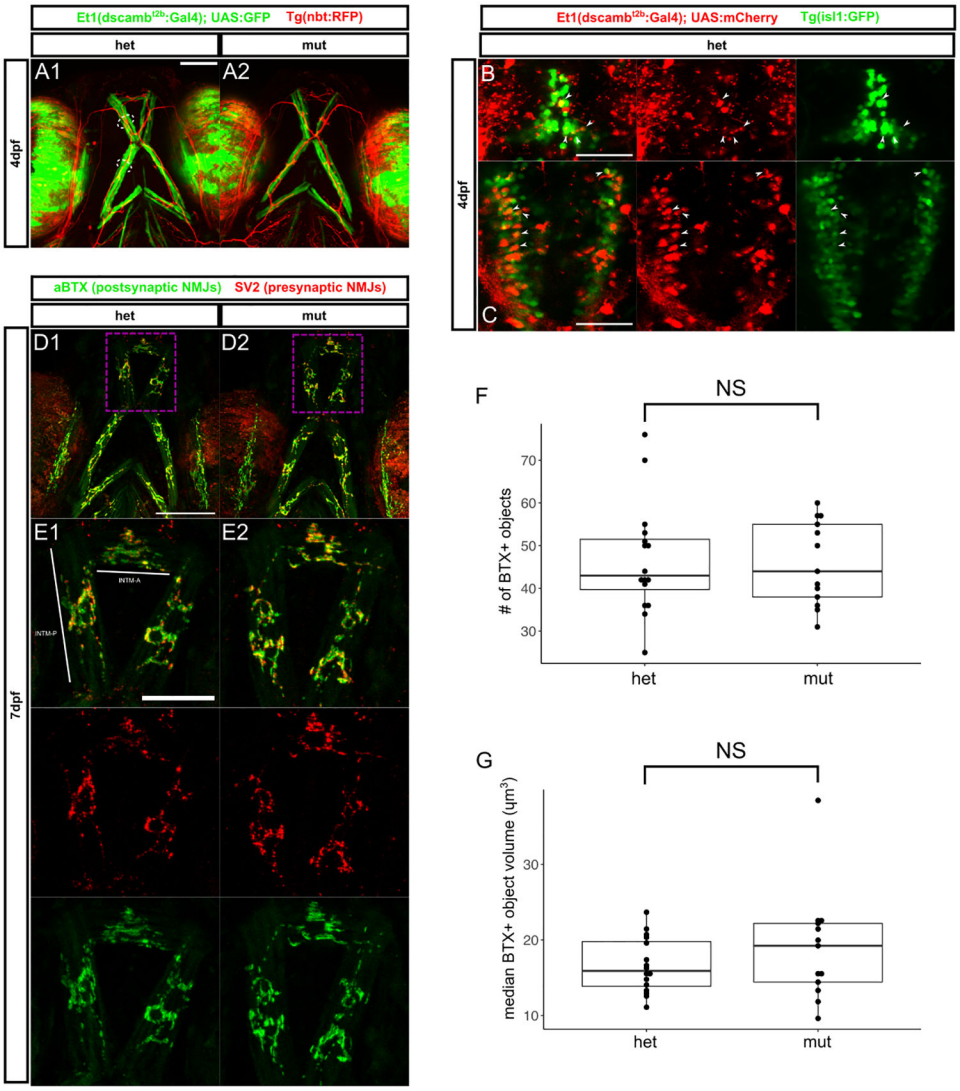

Figure 4 –. Jaw muscle fibers and branchiomotor innervation are intact in *dscamb* mutants

A) Ventral view of head in 4dpf larvae with Et1(dscamb^{t2b}:Gal4) expression in jaw muscle fibers in heterozygous (A1) and homozygous (A2) mutants. Arrowheads: BMN axons, dotted lines: jaw muscle fibers (MFs). Scale bar: 100µm

B, C) Dorsal images of hindbrain regions in 4dpf larvae with Et1(dscamb^{t2b}:Gal4) in red and BMNs in green [Tg(isl1:GFP)]. Confocal projections of the facial (B) and vagal (C) BMN nuclei. Arrowheads: examples of mCherry+/GFP+ BMNs. Scale bars: 50µm

D) Confocal projections of ventral head in 7dpf heterozygous (D1, E1) and homozygous (D2, E2) mutants with NMJs labeled presynaptically (SV2, red) and postsynaptically (aBTX, green). E1, E2 are magnifications of dashed boxes in D1, D2, showing NMJs on the INTM-A and INTMP muscles. Scale bar D1: 100µm, scale bar E1: 50µm

F, G) Quantification of aBTX-stained object number (F) and median volume on the INTM-A and INTM-P of 7dpf heterozygous and homozygous mutant larvae. N = 16 hets and 13 muts. Mann-Whitney-Wilcoxon test: p = 0.98 for F and p = 0.46 for G.

Middle line is the median; lower and upper ends of boxes are 25th and 75th percentiles.

Author Manuscript Author Manuscript Author Manuscript Author Manuscript

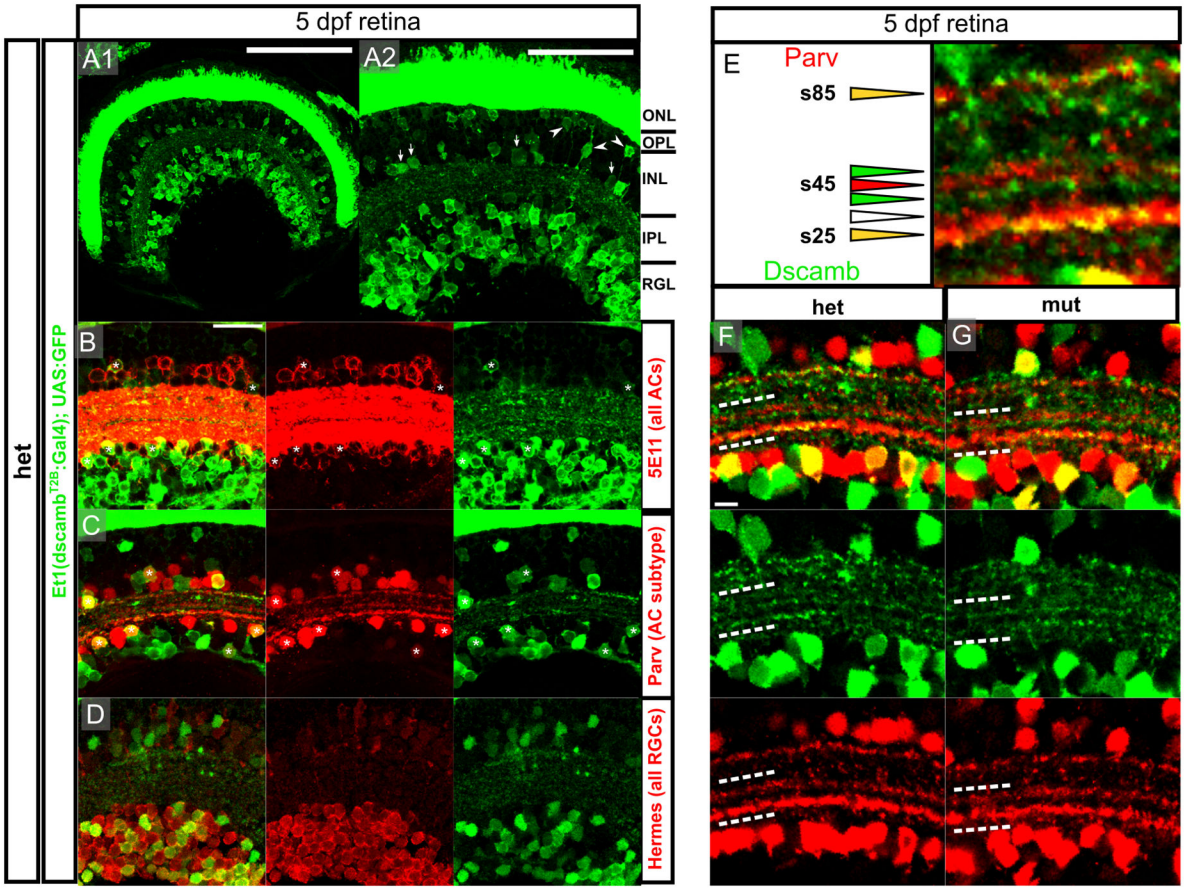

Figure 5 –. *dscamb* is expressed in ACs and RGCs subtypes, but is not required for IPL lamination

A1) Et1(dscamb^{t2b}:Gal4) expression in retinal section from 5dpf larva. Dorsal is left, medial is up. Scale bars: 100μm.

A2) Higher magnification image of A1. Arrowheads: BCs, arrows: ACs. ONL: outer nuclear layer, OPL: outer plexiform layer, INL: inner nuclear layer, IPL: inner plexiform layer, RGL: retinal ganglion cell layer. Scale bar: 50μm.

B-D) Confocal images of IPL in sections from 5dpf heterozygous larvae. Scale bar: 20μm.

B) Et1(dscamb^{t2b}:Gal4) compared to pan-AC marker (5E11; red). Asterisks: GFP+/5E11+ ACs.

C) Et1(dscamb^{t2b}:Gal4) compared to Parv+ AC marker (red). Asterisks: GFP+/Parv+ ACs.

D) Et1(dscamb^{t2b}:Gal4) compared to pan-RGC marker (Hermes; red).

E) s25, s45, and s85 Parv+ sublaminae in the IPL. Triangles indicate sublaminae that are GFP+/Parv+ (yellow), GFP+ only (green), Parv+ only (red), or negative for both (empty). Scale bar: 5um.

F,G) Images of IPL in 5dpf heterozygous (F) and homozygous (G) *dscamb* mutant larvae. White dashed lines outline region containing s25 and s45 Parv+ sublaminae. Scale bar: 5um.

Author Manuscript Author Manuscript Author Manuscript Author Manuscript

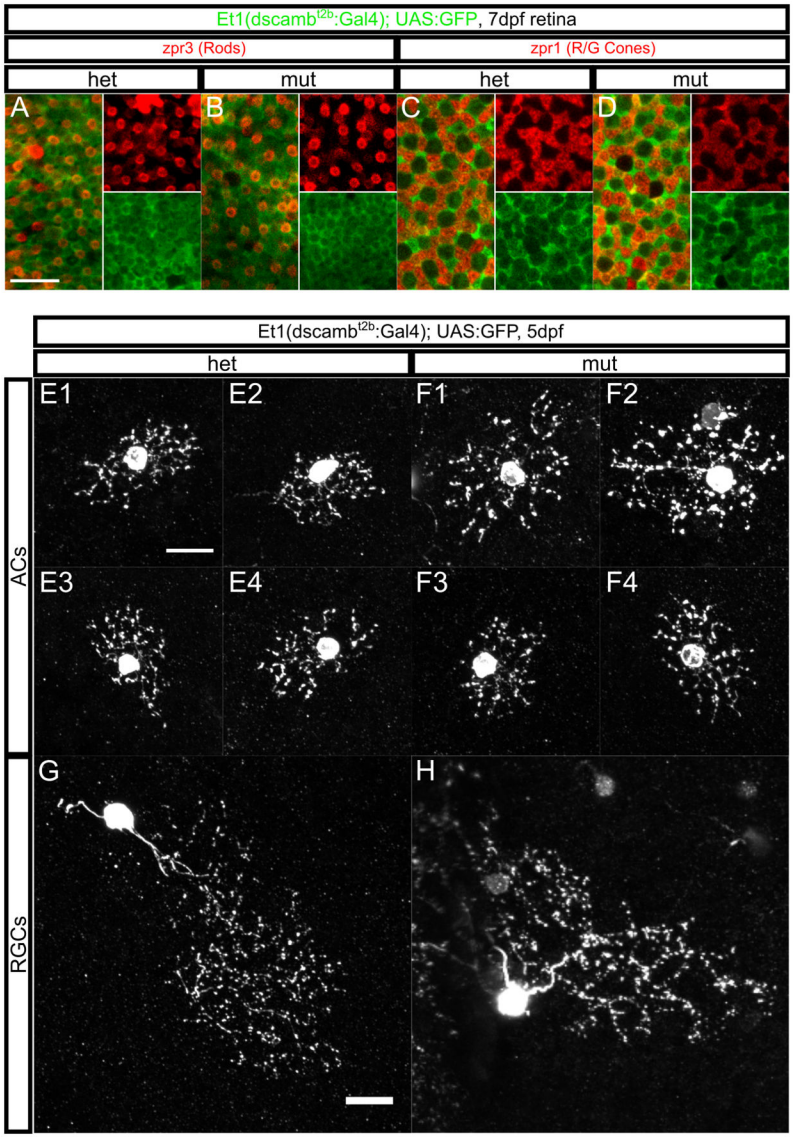

Figure 6 –. *dscamb* is not required for PR mosaic spacing or RGC/AC self-avoidance

A-D) Confocal projection through the base of zpr3+ rod outer segments (red A,B) or zpr1+ R/G cone cell bodies (red C,D) in retinas from 7dpf heterozygous (A, C) and homozygous (B, D) *dscamb* mutant larvae. Et1(dscamb^{t2b}:Gal4) expression is green. Insets on the right side of each panel are single-color continuations of the left side. Scale bar in A: 10μm.

E-H) Sparse Et1(dscamb^{t2b}:Gal4) labeling in individual ACs (E and F) or RGCs (G and H) in 5dpf heterozygous (E and G) and homozygous (F and H) dscamb mutant retinas. Scale bars: 10μm.

Author Manuscript Author Manuscript Author Manuscript Author Manuscript

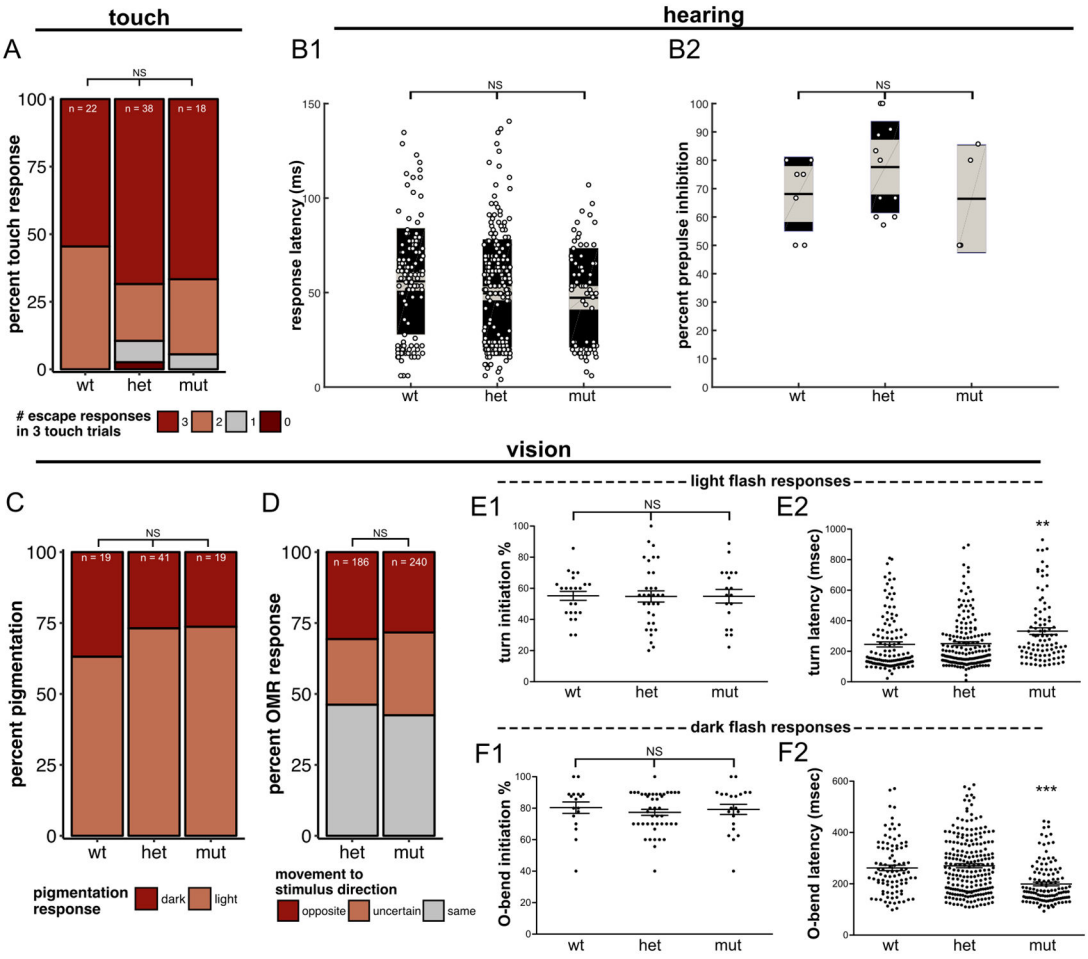

Figure 7 –. Sensory-evoked behavior in *dscamb* mutants

A) Percentage of 3 dpf wild-type, heterozygous, and homozygous *dscamb* mutant larvae responding with 0, 1, 2, or 3 escape behaviors in three 3 tail touch trials. Fisher's exact test of independence: p = 0.40.

B1) Auditory startle response latency in 6–8dpf larvae. Middle bar: mean. Grey boxes: 95% confidence intervals. Outer black boxes: one standard deviation. ANOVA: p = 0.46.

B2) Pre-pulse inhibition (PPI) of 6–8dpf larvae. ANOVA: p = 0.98.

C) Visually-mediated background adaptation. Percentage of 7dpf larvae that adapted pigmentation (light) or failed to adapt pigmentation (dark) to a bright background. Fisher's exact test: p = 0.72.

D) Optomotor response (OMR). Percentage of trials in which 7dpf heterozygous and homozygous mutant *dscamb* larvae responded to a rotating visual stimulus by moving in the same, opposite, or uncertain direction. 31 hetorozygous larvae were tested in 186 trials. 40 mutant larvae were tested in 240 trials. Fisher's exact test of independence: p = 0.39.

E, F) Light (E) and dark (F) flash responses. Light flashes elicit turning responses and dark flashes elicit O-bends. The percentage of trials with responses (E1, F1) and response latency during individual trials for each 5dpf larva (E2, F2). Error = SEM. ANOVA: **p < 0.01, ***p<0. N ≥ 17 animals, ≥ 94 responses for each experiment.

Author Manuscript Author Manuscript Author Manuscript Author Manuscript

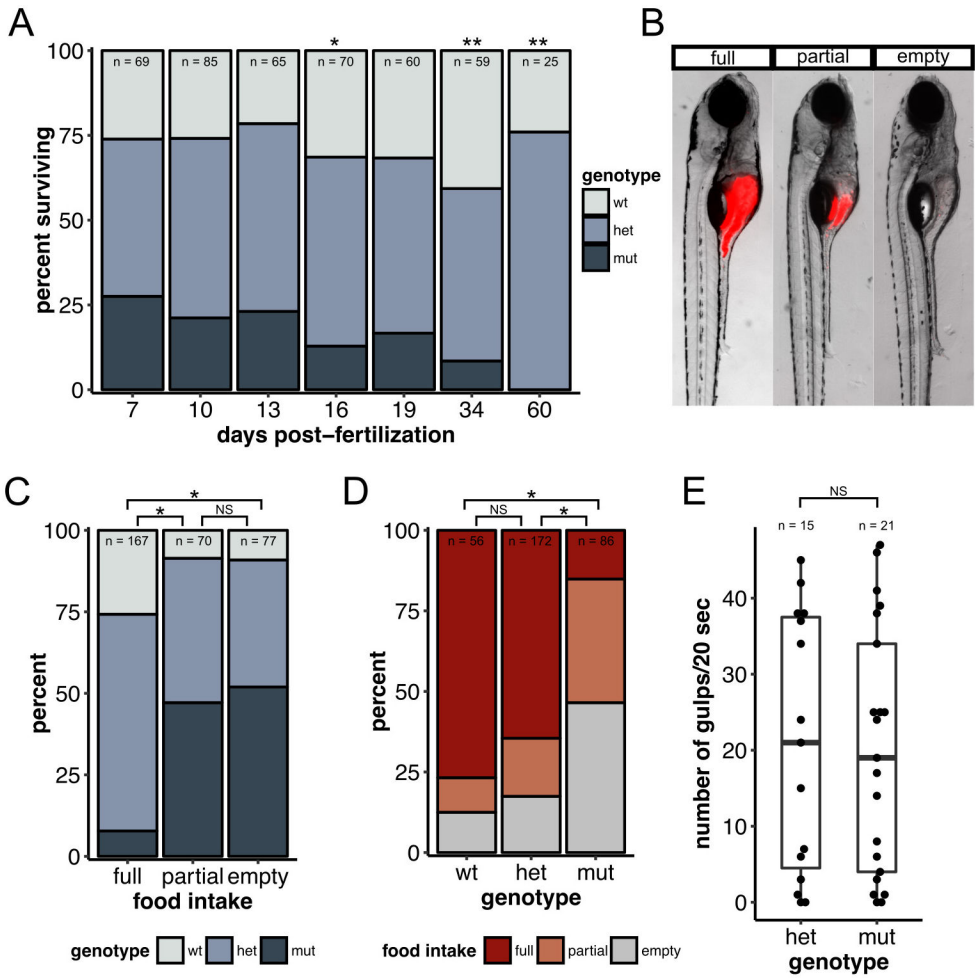

Figure 8 –. *dscamb* mutants have defective feeding behavior and die at 2–3 weeks of age

A) Percentage of offspring of each genotype from heterozygous *dscamb* mutant crosses that survived to different time points. Multinomial exact test for goodness-of-fit (predicted proportions wt:het:mut = 0.25:0.75:0.25) p-value: 7dpf = 0.80, 10dpf =0.74, 13dpf =0.73, 16dpf =0.046, 19dpf =0.25, 34dpf =0.0013, 60dpf =0.0017.

B) Representative images of 7dpf larvae in three categories of fluorescent food intake.

C) Percentage of each genotype in each food intake category. Fisher's exact test of independence across all groups: p = 0.00050. Post-hoc Fisher's exact test with Bonferroni correction: full × partial p = 1.2e-10, full × empty p = 4.1e-13, partial × empty p = 1.0.

D) Percentage of each food intake category in each genotype. Fisher's exact test of independence across all groups: p = 0.00050. Post-hoc Fisher's exact test with Bonferroni correction: wt × het p = 0.81, wt × mut p = 2.2e-12, het × mut p = 1.8e-13.

E) Quantification of number of gulps during a 20sec movie for 7dpf heterozygous and homozygous mutants. Each data point represents one fish. Mann-Whitney-Wilcoxon test: p = 0.99. Middle line is the median; lower and upper ends of boxes are 25th and 75th percentiles.